

Highly controllable and robust 2D Spin-Orbit Coupling for quantum gases

Wei Sun,^{1,2} Bao-Zong Wang,^{1,2,3,4} Xiao-Tian Xu,^{1,2} Chang-Rui Yi,^{1,2} Long Zhang,^{3,4}
Zhan Wu,^{1,2} Youjin Deng,^{1,2} Xiong-Jun Liu,^{3,4,*} Shuai Chen,^{1,2,†} and Jian-Wei Pan^{1,2,‡}

¹*Shanghai Branch, National Research Center for Physical Sciences at Microscale and Department of Modern Physics, University of Science and Technology of China, Shanghai 201315, China*

²*Chinese Academy of Sciences Center for Excellence: Quantum Information and Quantum Physics, University of Science and Technology of China, Hefei Anhui 230326, China*

³*International Center for Quantum Materials, School of Physics, Peking University, Beijing 100871, China*

⁴*Collaborative Innovation Center of Quantum Matter, Beijing 100871, China*

We report the realization of a robust and highly controllable two-dimensional (2D) spin-orbit (SO) coupling with topological non-trivial band structure. By applying a retro-reflected 2D optical lattice, phase tunable Raman couplings are formed into the anti-symmetric Raman lattice structure, and generate the 2D SO coupling with precise inversion and C_4 symmetries, leading to considerably enlarged topological regions. The life time of the 2D SO coupled Bose-Einstein condensate reaches several seconds, which enables the exploring of fine tuning interaction effects. These essential advantages of the present new realization open the door to explore exotic quantum many-body effects and non-equilibrium dynamics with novel topology.

Spin-orbit (SO) coupling, as a fundamental quantum effect, is an essential ingredient in many topological phases of quantum matter, including the topological insulators [1, 2] and topological semimetals [3–6]. In the field of ultracold atoms which can offer extremely clean and controllable platforms for quantum simulation, synthetic SO coupling schemes were proposed [7–11] via light-atom interactions which flip atomic spins and transfer momentum simultaneously. The 1D SO coupling has now been realized routinely in the experiments for both ultracold bosons [12, 13] and fermions [14, 15] as continuum atom gases or trapped in optical lattices [16, 17]. Great interests have been drawn in emulating SO effects [18–24] and topological phases with ultracold atoms [25–38]. In particular, the simulation of broad classes of topological quantum states or phase transitions with quantum gases necessitates to synthesize 2D or higher dimensional SO couplings.

The 2D SO couplings with nontrivial band topology were recently realized for ⁸⁷Rb Bose-Einstein condensate (BEC) [39] and ⁴⁰K Fermi gases [40, 41]. However, they suffer from the instability of optical lattices with long loop lines [34, 39] or heating with complex Raman couplings between multiple ground states [40, 41]. These shortcomings make it hard to explore the exotic topological quantum phases with high precision. Realization of 2D SO coupled atom gas with high controllability and long lifetime, which are essential for quantum simulations of exotic states, are highly desired.

In this Letter, we report on the synthesis of a 2D SO coupling with high controllability, stability, and long lifetime. The realization is based on a new optical Raman lattice scheme [42], with the optical instability and heating in the previous works [39–41] all being overcome. The 2D SO coupling exhibits precise inversion and C_4 symmetries, which are the key features and bring important new physics, including a highly resolved crossover between 1D

and 2D SO couplings, a long lifetime of the 2D SO coupled BEC up to several seconds, one order of magnitude longer than those in Refs. [39–41], the detection with high precision of the critical transition point from stripe phase to plane-wave phases [12, 43], and the considerably broadened topological regions. This work paves the way for further studies of quantum many-body physics and quantum non-equilibrium dynamics with novel topology.

The new scheme of the 2D SO coupling [42] with ultracold ⁸⁷Rb atoms is illustrated in Fig.1(a). The 2D square lattice $V_{\text{latt}}(x, y)$ is constructed with two linear polarized laser beams \mathbf{E}_x and \mathbf{E}_y (the blue and red lines in Fig. 1(a)), with wavelength of $\lambda = 787\text{nm}$ (wave vector $k_0 = 2\pi/\lambda$ and recoil energy $E_r = \hbar^2 k_0^2 / 2m$). The beams pass through $\lambda/2$ waveplates to generate two orthogonally polarized components E_{xz} (E_{yz}) and E_{xy} (E_{yx}) before shining on the atoms. The key setting is that they are retro-reflected back by two mirrors (R_x and R_y) to form a 2D square lattice, where two $\lambda/4$ wave-plates with optical axis along \hat{z} direction are placed in front of the mirrors as the phase retarders to generate π phase delay between the two orthogonal polarization components. The 2D lattice potential then reads

$$V_{\text{latt}}(x, y) = V_{0x} \cos^2 k_0 x + V_{0y} \cos^2 k_0 y, \quad (1)$$

with lattice depth $V_{0x(y)} \propto |E_{xy(yx)}|^2 - |E_{xz(yz)}|^2$ [42, 44]. We tune $V_{0x} = V_{0y} = V_0$ to have a symmetric 2D lattice.

The spin up/down states are defined via two magnetic sub-levels in $F = 1$ manifold, i.e. $|1, -1\rangle$ and $|1, 0\rangle$. A bias magnetic field \mathbf{B} of 14.5G is applied in \hat{z} -direction, giving a Zeeman split of 10.2MHz. The $|1, 1\rangle$ state is effectively suppressed due to the large quadratic Zeeman shift ($\epsilon \approx 8.2E_r$). The Raman couplings are generated by the orthogonal polarization pairs (E_{xz}, E_{yx}) and (E_{xy}, E_{yz}) , respectively, realizing the double- Λ configuration, with $\Omega_1 = \Omega_{01} \sin k_0 x \cos k_0 y$ and $\Omega_2 = \Omega_{02} \cos k_0 x \sin k_0 y$, shown in Fig. 1(b). The coupling strength $\Omega_{01} \propto$

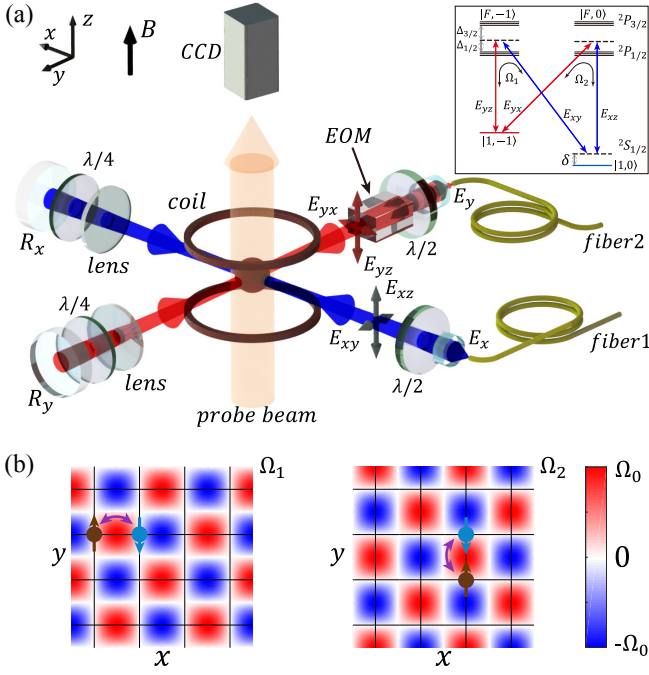


Figure 1. (a) Experimental setup. The \mathbf{B} field along z -axis generates the Zeeman splitting and the quantization axis of the atoms. The red and blue lines are lasers to construct the 2D lattice and Raman couplings. The $\lambda/2$ -waveplates are used to generate two orthogonal polarization components of the lattices. The $\lambda/4$ -waveplates are phase retarders, which are applied to form the anti-symmetric Raman coupling lattices. The EOM is applied to tune the relative phase $\delta\varphi$ between two Raman couplings Ω_1 and Ω_2 . insets: level structure and Raman coupling scheme. (b) The anti-symmetric structure of the two Raman couplings Ω_1 and Ω_2 in real space. The grid represent the square optical lattice $V_{\text{latt}}(x, y)$.

$|E_{yz}||E_{xy}|$ and $\Omega_{02} \propto |E_{yx}||E_{xz}|$ [42, 44]. Due to the anti-symmetric lattice structure, the onsite Raman coupling vanishes. Only in the tunneling, the atoms experience non-zero coupling strength which causes the spin-flip Raman diffraction. This is essential for the generation of non-trivial topological band structure in the 2D SO coupling system [39, 42]. An electro-optical phase modulator (EOM) is placed in one of the beam path to tune the relative phase $\delta\varphi$ between Ω_1 and Ω_2 . The total Raman coupling term reads

$$\Omega_R(x, y) = \begin{pmatrix} 0 & \Omega_1 + e^{i\delta\varphi}\Omega_2 \\ \Omega_1^* + e^{-i\delta\varphi}\Omega_2^* & 0 \end{pmatrix} \quad (2)$$

We adjust the two $\lambda/2$ waveplates to set $\Omega_{01} = \Omega_{02} = \Omega_0$ so that $\Omega_R(x, y)$ satisfies reflective anti-symmetry. An optimal 2D SO coupling is achieved with $\delta\varphi = \pm\pi/2$.

In this scheme, the initial and propagation phases of the laser beams are static global phases and can be neglected [42, 44]. The total Hamiltonian reads

$$\hat{H} = \frac{\mathbf{p}^2}{2m} + V_{\text{latt}}(x, y) + \Omega_R(x, y) + \frac{\delta}{2}\sigma_z, \quad (3)$$

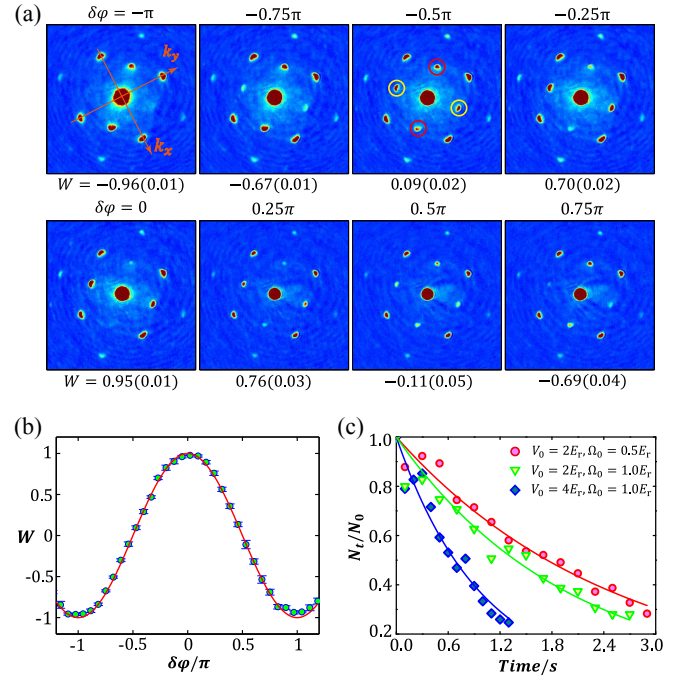


Figure 2. (a) TOF image of the SO coupled BEC with various phases $\delta\varphi$. The images with $\delta\varphi = -\pi, 0$ correspond to 1D SO coupling, and those with $\delta\varphi = \pm\pi/2$ are for symmetric 2D SO coupling. (b) W versus $\delta\varphi$. The blue circles are experimental data, with the error bar for the standard statistical error. The red solid line is the theoretical curve without fitting. (c) The measured life time τ of 2D SO coupled BEC with $\delta\varphi = \pi/2$. By fitting with an exponential decay, we obtain the lifetime as $\tau = 2.52 \pm 0.07\text{s}$ (red line), $2.00 \pm 0.09\text{s}$ (green line) and $0.980 \pm 0.05\text{s}$ (blue line).

where m is the atomic mass, δ is the two-photon Raman detuning. It is the realization of a minimal quantum anomalous Hall (QAH) model driven by the SO coupling [34]. Different from the previous realization of 2D SO coupling [39], this Hamiltonian has the precise inversion and C_4 symmetries, which lead to nontrivial physics as presented below.

Properties of 2D SO coupled BEC. The BEC with 3.0×10^5 ^{87}Rb atoms is prepared in $|1, -1\rangle = |\uparrow\rangle$ state. The 2D lattice and Raman coupling beams are ramped up adiabatically in 80ms, and the BEC is loaded into the ground state of the Hamiltonian (Eq. 3) with $V_0 = 4.0E_r$, $\Omega_0 = 1.0E_r$ and $\delta = 0$. By manipulating the voltage on the EOM, we can tune $\delta\varphi$ continuously over 2π range, which governs the interference of the Raman couplings $\Omega_{1,2}$ [44] and leads to the crossover between 1D and 2D SO couplings. For detection, a time-of-flight (TOF) image is taken after the BEC is free released for 25ms.

A highly resolved crossover between 1D and 2D SO couplings is observed in Fig. 2(a,b). The major atom cloud in $|\uparrow\rangle$ state stays at momentum $(k_x, k_y) = (0, 0)$. The four atom clouds with momenta $\mathbf{k} = (\pm k_0, \pm k_0)$ in diagonal and off-diagonal directions are in $|\downarrow\rangle$ state

diffracted by the Raman coupling term. As shown in Fig.2(a), the distribution of the four $|\downarrow\rangle$ atom clouds varies versus $\delta\varphi$, which characterize the interference of the Raman coupling lattices Ω_1 and Ω_2 . We define $W(\delta\varphi)$ to quantify this interference by

$$W(\delta\varphi) = \frac{N_{\hat{x}+\hat{y}} - N_{\hat{x}-\hat{y}}}{N_{\hat{x}+\hat{y}} + N_{\hat{x}-\hat{y}}}, \quad (4)$$

where $N_{\hat{x}+\hat{y}}$ ($N_{\hat{x}-\hat{y}}$) is the total number of atoms in the diagonal (off-diagonal) direction, as denoted by red (yellow) circles in Fig. 2(a), For the 1D SO coupling with $\delta\varphi = \pi$ (0), the Raman diffracted atoms are only in the diagonal (off-diagonal) direction, and we have $W = -0.96 \pm 0.01$ (0.95 ± 0.01). For the optimal 2D SO coupling with $\delta\varphi = \pm\pi/2$, the Raman diffracted atoms are almost evenly distributed, and we obtain $W = -0.11 \pm 0.05$ and 0.09 ± 0.02 . In comparison with Ref. [39], the quality of Fig. 2(a,b) is significantly improved.

Further, the lifetime of the BEC with 2D SO coupling ($\delta\varphi = \pi/2$) is measured. After adiabatically loading the condensate, we measure the normalized number of condensate atoms $N(t)/N(0)$ as a function of the holding time t . The results, shown in Fig. 2(c) for different lattice depths V_0 and Raman coupling strength Ω_0 , are fitted to an exponential function $e^{-t/\tau}$. We obtain the lifetime $\tau = 0.980 \pm 0.05\text{s}$ for $(V_0, \Omega_0) = (4.0, 1.0)E_r$, $2.00 \pm 0.09\text{s}$ for $(4.0, 2.0)E_r$, and $2.52 \pm 0.07\text{s}$ for $(2.0, 0.5)E_r$. Compared to Refs. [39–41], the lifetime of quantum gas is enhanced over one order of magnitude.

Ground state phase transition. The high controllability, stability, and especially the long lifetime of the present 2D SO coupling, make it feasible to study the ground state phase transition driven by interaction, for which the longtime relaxation is essential for the system to reach the equilibrium [12, 43]. In particular, we measure the stripe phase (ST) and magnetic phase (MG) of the ground state for the present 2D SO coupled BEC (with $\delta\varphi = \pi/2$) [45]. To observe and distinguish the two phases, the magnetization M_0 is defined as [43],

$$M_0 = \frac{N_{0\uparrow} - N_{0\downarrow}}{N_{0\uparrow} + N_{0\downarrow}}, \quad (5)$$

where $N_{0\uparrow}$ ($N_{0\downarrow}$) represents the number of condensate atoms in the $|\uparrow\rangle$ ($|\downarrow\rangle$) state. In this measurement, 10^6 atoms right above the BEC critical temperature, with half-and-half spin states, are loaded adiabatically into the 2D SO coupled system with fixed ($V_0 = 2.0E_r$, $\delta = 0$) and variable Ω_0 . The atoms are further cooled to pure condensate in 800ms and held for another 1.5s for relaxing to equilibrium before detection. Finally, the spin-resolved TOF image is taken to measure $N_{0\uparrow}$ and $N_{0\downarrow}$.

We repeat the measurement hundreds of times at every Ω_0 . Each value of M_0 is recorded to obtain the histograms for statistical analysis as shown in Fig. 3(a). For very small Ω_0 (as $0.04E_r$ and $0.02E_r$), the histogram

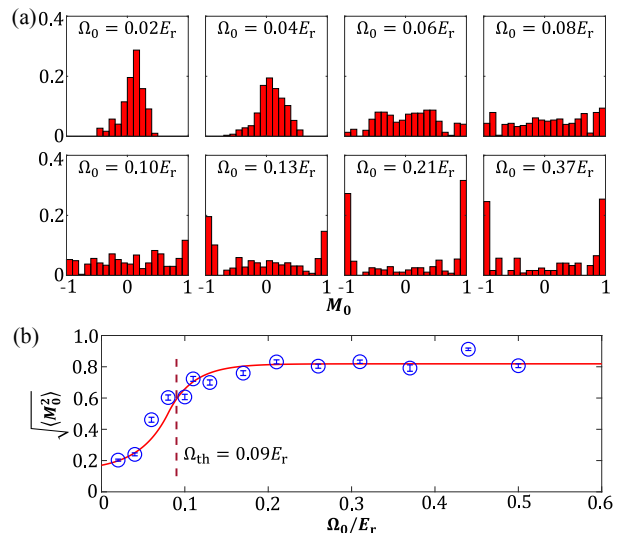


Figure 3. Phase transition of the 2D SO coupled BEC between the ST and the MG phase. (a) Magnetization histograms with varying Ω_0 for nearly pure condensate. (b) $\sqrt{\langle M_0^2 \rangle}$ as a function of Ω_0 . The error bars give the standard statistical errors. The red solid line is an arbitrary fit. The dashed line shows the theoretical calculation of phase transition point.

of the magnetization shows a single peak centered at $M_0 \approx 0$, corresponding to the ST phase. For larger Ω_0 (as $0.21E_r$ and $0.37E_r$), the histogram of M_0 shows two sharp peaks close to ± 1 , giving the MG phase [43]. In contrast to the ideal thermodynamic case which would exhibit an infinitely sharp transition between the two- and single-peak structures, the histogram broadens and flattens gradually in the moderate regime (from $\Omega_0 = 0.06E_r$ to $0.10E_r$). This is due to the very small energy difference between the ST and MG states near the phase transition point, which leads to very long relaxation time to reach the equilibrium and domains with various sizes may form during the relaxation (see Supplementary Materials (SM) for details, which include Ref. [49]).

The phase transition is determined from the turning point in the plot of $\sqrt{\langle M_0^2 \rangle}$ versus Ω_0 (Fig. 3(b)). The fit gives the critical point as $\Omega_c = 0.08 \pm 0.02E_r$, consistent with the theoretical prediction $\Omega_{\text{th}} = 0.09E_r$ [45]. The experimental determination of Ω_c , which is difficult in Ref. [39], shows the feasibility of the present realization for exploring many-body effects.

Extended topological region. We proceed to measure the band topology, with $\delta\varphi = \pi/2$ [42]. The topology of the s -band can be determined directly by the product of the signs of the spin-polarizations at the four symmetric momenta $\{\Lambda_j\} = \{\Gamma(0,0), X_1(0,\pi), X_2(\pi,0), M(\pi,\pi)\}$ in the FBZ [46]. At low temperature regime, only the s -band is effectively populated. The measured spin-polarization $P(\mathbf{q})$ is dominated by the spin-polarization in the lowest s -band $P_0(\mathbf{q})$. Then we have

$$\Theta = \prod_{j=1}^4 \text{sgn}[P(\Lambda_j)], \quad (6)$$

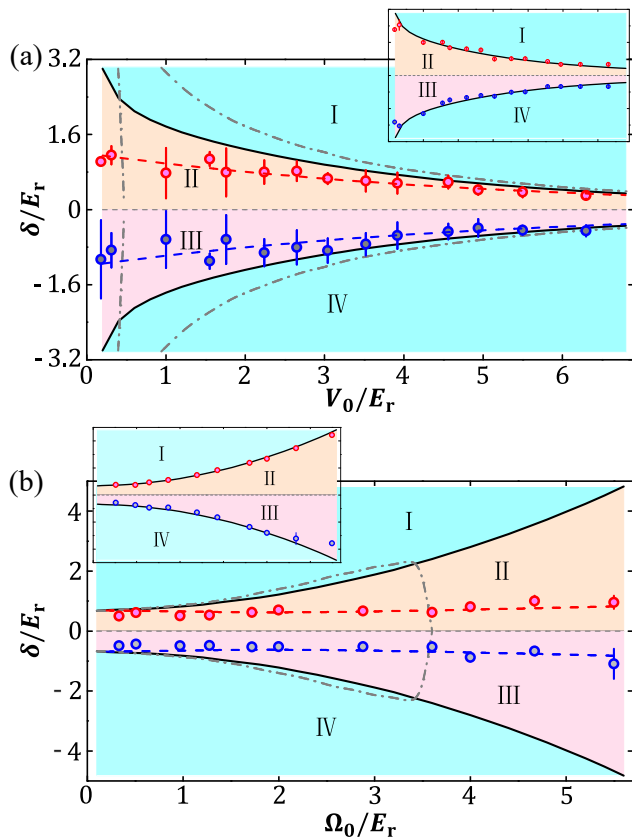


Figure 4. Topological phase diagram of the lowest band. The regions I and IV are trivial with the Chern number $\mathcal{C}_1^{(0)} = 0$. The areas II and III are topological non-trivial with $\mathcal{C}_1^{(0)} = \pm 1$, respectively. The black solid lines are the topological phase boundaries in the present scheme, and the gray dash-dot lines are that of asymmetric Raman coupling in Ref. [39]. The circles with statistical error bars are the phase boundaries measured in the experiment. (a) $\delta - V_0$ plane with $\Omega_0 = 0.5E_r$. (b) $\delta - \Omega_0$ plane with $V_0 = 4.0E_r$. The measurements deviate from the calculation at small V_0 and large Ω_0 , due to the higher band and heating effects. Insets: by considering the thermal effect and removing the high-band contribution from the experimental data, the phase boundaries are found to be fit to the theoretical calculation.

with the topologically trivial and non-trivial phases corresponding to $\Theta = 1$ and -1 , respectively [46]. The Chern number of the lowest band is then obtained as

$$\mathcal{C}_1^{(0)} = -\frac{1 - \Theta}{4} \sum_{j=1}^4 \text{sgn}[P(\Lambda_j)]. \quad (7)$$

In the experiment, about 2.0×10^5 thermal atoms at temperature 100nK are filled into the lowest band, with the higher band population being relatively small. The spin-resolved TOF imaging measures the atom densities at spin-up ($n_{\uparrow}(\mathbf{q})$) and spin-down ($n_{\downarrow}(\mathbf{q})$) in momentum space. The spin-polarization at quasi-momentum \mathbf{q} is obtained as $P(\mathbf{q}) = [n_{\uparrow}(\mathbf{q}) - n_{\downarrow}(\mathbf{q})] / [n_{\uparrow}(\mathbf{q}) + n_{\downarrow}(\mathbf{q})]$. By varying δ , we take each of the $P(\Lambda_j)$ to calculate $\Theta(\delta)$

and obtain the topological phase boundary (see the SM for details). The experimental results (circles) and numerical simulation (solid lines) are shown in Fig. 4, for the $\delta - V_0$ plane with fixed $\Omega_0 = 0.5E_r$ [for (a)] and for the $\delta - \Omega_0$ plane with fixed $V_0 = 4.0E_r$ [for (b)]. The regions II and III (I and IV) are for topological (trivial) bands with $\mathcal{C}_1^{(0)} = \pm 1$ ($\mathcal{C}_1^{(0)} = 0$). The Chern number changes sign when δ crosses zero. The topological region extends to the limit $V_0 \rightarrow 0$ (a) and $\Omega_0 \rightarrow \infty$ (b), as predicted in Ref. [42]. This is in sharp contrast to the case without C_4 symmetry [39?] $V_0^c \approx 0.46E_r$ and $\Omega_0^c \approx 3.6E_r$, respectively. The broad topological region with weak lattice limit $V_0 \rightarrow 0$ can enable to explore topological physics in nearly continuous regimes.

The directly measured phase boundaries in Fig. 4 are narrower than those predicted in theory for the following two reasons. First, as V_0 decreases and/or Ω_0 increases, the system gradually deviates from the tight-binding condition. The high-band effect suppresses the net magnitudes of spin-polarizations $P(\Lambda_j)$ at symmetric momenta. Second, the heating becomes serious for large Ω_0 (e.g. for $\Omega_0 = 4.65E_r$, the temperature of the atoms increases from 100nK to nearly 300nK). These effects reduce the resolution of s -band spin-polarization due to the high-band population. Subtracting such high-band contribution from the measured total spin-polarization we can obtain the spin-polarization contributed only from the lowest-band states (see the SM for details). We then recalculate the topological index and find that the results agree well with the numerical solution (the insets of Fig.4).

In conclusion, we have synthesized a highly controllable and robust 2D SO coupling for quantum gases via an anti-symmetric Raman lattice scheme. It exhibits precise inversion and C_4 symmetries. The lifetime of the 2D SO coupled BEC reaches several seconds, which enable us to study the delicate interaction-driven ground state phase transition where long time relaxation is required. Further, the precise symmetries qualitatively enlarge the topological region in the phase diagram, and leads to topological bands with arbitrary Raman coupling strength and lattice depth. Moreover, the present scheme can be also applied to other Bosonic or Fermionic quantum gases systems. As for ^{40}K , the estimated heating is about 5 times larger than that of ^{87}Rb , giving a life time of hundreds of milliseconds (see SM which include Ref. [50]). It is thus expected that rich quantum many-body phenomena with non-trivial topology can be also studied in 2D SO coupled fermionic systems. The high controllability and stability of the 2D SO coupling open intriguing opportunities to explore novel topological quantum effects and far-from-equilibrium quantum dynamics with topology.

We thank J. -S Pan and W. Yi for the helpful discussion. This work was supported by the National Key R&D Program of China (under grants 2016YFA0301601 and

2016YFA0301604), National Nature Science Foundation of China (under grants NO. 11674301, No. 11574008, No. 11761161003, and No. 11625522), and the Thousand-Young-Talent Program of China.

* xiongjunliu@pku.edu.cn

† shuai@ustc.edu.cn

‡ pan@ustc.edu.cn

- [1] M. Z. Hasan and C. L. Kane, *Colloquium: Topological Insulators*, Rev. Mod. Phys. **82**, 3045 (2010).
- [2] X.-L. Qi and S.-C. Zhang, *Topological Insulators and Superconductors*, Rev. Mod. Phys. **83**, 1057 (2011).
- [3] X. Wan, A. M. Turner, A. Vishwanath, and S. Y. Savrasov, *Topological Semimetal and Fermi-Arc Surface States in the Electronic Structure of Pyrochlore Iridates*, Phys. Rev. B **83**, 205101 (2011).
- [4] A. A. Burkov and L. Balents, *Weyl Semimetal in a Topological Insulator Multilayer*, Phys. Rev. Lett. **107**, 127205 (2011).
- [5] S.-Y. Xu, I. Belopolski, N. Alidoust, M. Neupane, G. Bian, C. Zhang, R. Sankar, G. Chang, Z. Yuan, C.-C. Lee, S.-M. Huang, H. Zhang, J. Ma, D. S. Sanchez, B. Wang, A. Bansil, F. Chou, P. P. Shibayev, H. Lin, S. Jia, and M. Z. Hasan, *Discovery of a Weyl Fermion Semimetal and Topological Fermi Arcs*, Science **349**, 613 (2015).
- [6] B. Q. Lv, H. M. Weng, B. B. Fu, X. P. Wang, H. Miao, J. Ma, P. Richard, X. C. Huang, L. X. Zhao, G. F. Chen, Z. Fang, X. Dai, T. Qian, and H. Ding, *Experimental Discovery of Weyl Semimetal TaAs*, Phys. Rev. X **5**, 031013 (2015).
- [7] K. Osterloh, M. Baig, L. Santos, P. Zoller, and M. Lewenstein, *Cold Atoms in Non-Abelian Gauge Potentials: From the Hofstadter "Moth" to Lattice Gauge Theory*, Phys. Rev. Lett. **95**, 010403 (2005).
- [8] J. Ruseckas, G. Juzeliūnas, P. Öhberg, and M. Fleischhauer, *Non-Abelian Gauge Potentials for Ultracold Atoms with Degenerate Dark States*, Phys. Rev. Lett. **95**, 010404 (2005).
- [9] X.-J. Liu, H. Jing, X. Liu, and M.-L. Ge, *Generation of Two-Flavor Vortex Atom Laser from a Five-State Medium*, Eur. Phys. J. D **37**, 261 (2005); arXiv:quant-ph/0410096.
- [10] T. D. Stanescu, C. Zhang, and V. Galitski, *Nonequilibrium Spin Dynamics in a Trapped Fermi Gas with Effective Spin-Orbit Interactions*, Phys. Rev. Lett. **99**, 110403 (2007).
- [11] X.-J. Liu, M. F. Borunda, X. Liu, and J. Sinova, *Effect of Induced Spin-Orbit Coupling for Atoms via Laser Fields*, Phys. Rev. Lett. **102**, 046402 (2009).
- [12] Y.-J. Lin, K. Jiménez-García, and I. B. Spielman, *Spin-Orbit-Coupled Bose-Einstein Condensates*, Nature (London) **471**, 83 (2011).
- [13] J.-Y. Zhang, S.-C. Ji, Z. Chen, L. Zhang, Z.-D. Du, B. Yan, G.-S. Pan, B. Zhao, Y.-J. Deng, H. Zhai, S. Chen, and J.-W. Pan, *Collective Dipole Oscillations of a Spin-Orbit Coupled Bose-Einstein Condensate*, Phys. Rev. Lett. **109**, 115301 (2012).
- [14] P. Wang, Z.-Q. Yu, Z. Fu, J. Miao, L. Huang, S. Chai, H. Zhai, and J. Zhang, *Spin-Orbit Coupled Degenerate Fermi Gases*, Phys. Rev. Lett. **109**, 095301 (2012).
- [15] L. W. Cheuk, A. T. Sommer, Z. Hadzibabic, T. Yefsah, W. S. Bakr, and M. W. Zwierlein, *Spin-Injection Spectroscopy of a Spin-Orbit Coupled Fermi Gas*, Phys. Rev. Lett. **109**, 095302 (2012).
- [16] C. Qu, C. Hamner, M. Gong, C. Zhang, and P. Engels, *Observation of Zitterbewegung in a Spin-Orbit-Coupled Bose-Einstein Condensate*, Phys. Rev. A **88**, 021604(R) (2013).
- [17] C. Hamner, C. Qu, Y. Zhang, J. Chang, M. Gong, C. Zhang, and P. Engels, *Dicke-Type Phase Transition in a Spin-Orbit-Coupled Bose-Einstein Condensate*, Nat. Commun. **5**, 4023 (2014).
- [18] X.-J. Liu, X. Liu, L.-C. Kwek, and C. H. Oh, *Manipulating Atomic States via Optical Orbital Angular-Momentum*, Front. Phys. China, **3**, 113 (2008).
- [19] J. Dalibard, F. Gerbier, G. Juzeliūnas, and P. Öhberg, *Colloquium: Artificial Gauge Potentials for Neutral Atoms*, Rev. Mod. Phys. **83**, 1523 (2011).
- [20] N. Goldman, G. Juzeliūnas, P. Öhberg, and I. B. Spielman, *Light-Induced Gauge Fields for Ultracold Atoms*, Rep. Prog. Phys. **77**, 126401 (2014).
- [21] X. Zhou, Y. Li, Z. Cai, and C. Wu, *Unconventional States of Bosons with the Synthetic Spin-Orbit Coupling*, J. Phys. B: At. Mol. Opt. Phys. **46**, 134001 (2014).
- [22] H. Zhai, *Degenerate Quantum Gases with Spin-Orbit Coupling: a Review*, Rep. Prog. Phys. **78**, 026001 (2015).
- [23] F. Sun, J. Ye, W.-M. Liu, *Quantum magnetism of spinor bosons in optical lattices with synthetic non-Abelian gauge fields*, Phys. Rev. A **92**, 043609 (2015).
- [24] F. Sun, J. Ye, W.-M. Liu, *Quantum incommensurate skyrmion crystals and commensurate to incommensurate transitions in cold atoms and materials with spin-orbit couplings in a Zeeman field*, New J. Phys. **19**, 083015 (2017).
- [25] X.-J. Liu, X. Liu, L. C. Kwek, and C. H. Oh, *Optically Induced Spin Hall Effect in Atoms*, Phys. Rev. Lett. **98**, 026602 (2007).
- [26] S.-L. Zhu, H. Fu, C.-J. Wu, S.-C. Zhang, and L.-M. Duan, *Spin Hall Effects for Cold Atoms in a Light-Induced Gauge Potential*, Phys. Rev. Lett. **97**, 240401 (2006).
- [27] C. Zhang, S. Tewari, R. M. Lutchyn, and S. D. Sarma, *$p_x + ip_y$ Superfluid from s-Wave Interactions of Fermionic Cold Atoms*, Phys. Rev. Lett. **101**, 160401 (2008).
- [28] M. Sato, Y. Takahashi, and S. Fujimoto, *Non-Abelian Topological Order in s-Wave Superfluids of Ultracold Fermionic Atoms*, Phys. Rev. Lett. **103**, 020401 (2009).
- [29] X.-J. Liu, X. Liu, L. C. Kwek, and C. H. Oh, *Fractional Spin Hall Effect in Atomic Bose Gases*, Phys. Rev. B **79**, 165301 (2009).
- [30] N. Goldman, I. Satija, P. Nikolic, A. Bermudez, M. A. Martin-Delgado, M. Lewenstein, and I. B. Spielman, *Realistic Time-Reversal Invariant Topological Insulators with Neutral Atoms*, Phys. Rev. Lett. **105**, 255302 (2010).
- [31] S.-L. Zhu, L.-B. Shao, Z. D. Wang, and L.-M. Duan, *Probing Non-Abelian Statistics of Majorana Fermions in Ultracold Atomic Superfluid*, Phys. Rev. Lett. **106**, 100404 (2011).
- [32] C. Qu, Z. Zheng, M. Gong, Y. Xu, L. Mao, X. Zou, G. Guo, and C. Zhang, *Topological Superfluids with Finite-Momentum Pairing and Majorana Fermions*, Nat. Commun. **4**, 2710 (2013).
- [33] W. Zhang and W. Yi, *Topological Fulde-Ferrell-Larkin-*

- Ovchinnikov States in Spin-Orbit Coupled Fermi Gases*, Nat. Commun. **4**, 2711 (2013).
- [34] X.-J. Liu, K. T. Law, and T. K. Ng, *Realization of 2D Spin-Orbit Interaction and Exotic Topological Orders in Cold Atoms*, Phys. Rev. Lett. **112**, 086401 (2014).
- [35] Y. Xu and C. Zhang, *Berezinskii-Kosterlitz-Thouless Phase Transition in 2D Spin-Orbit-Coupled Fulde-Ferrell Superfluids*, Phys. Rev. Lett. **114**, 110401 (2015).
- [36] C. Chan and X.-J. Liu, *Non-Abelian Majorana Modes Protected by an Emergent Second Chern Number*, Phys. Rev. Lett. **118**, 207002 (2017).
- [37] Z. Gong, S. Higashikawa, and M. Ueda, *Zeno Hall Effect*, Phys. Rev. Lett. **118**, 200401 (2017).
- [38] C. Chan, L. Zhang, T. F. J. Poon, Y.-P. He, Y.-Q. Wang, and X.-J. Liu, *Generic Theory for Majorana Zero Modes in 2D Superconductors*, Phys. Rev. Lett. **119**, 047001 (2017).
- [39] Z. Wu, L. Zhang, W. Sun, X.-T. Xu, B.-Z. Wang, S.-C. Ji, Y. Deng, S. Chen, X.-J. Liu, and J.-W. Pan, *Realization of Two-Dimensional Spin-Orbit Coupling for Bose-Einstein Condensates*, Science **354**, 83 (2016).
- [40] L. Huang, Z. Meng, P. Wang, P. Peng, S.-L. Zhang, L. Chen, D. Li, Q. Zhou, and J. Zhang, *Experimental Realization of Two-Dimensional Synthetic Spin-Orbit Coupling in Ultracold Fermi Gases*, Nat. Phys. **12**, 540 (2016).
- [41] Z. Meng, L. Huang, P. Peng, D. Li, L. Chen, Y. Xu, C. Zhang, P. Wang, and J. Zhang, *Experimental Observation of a Topological Band Gap Opening in Ultracold Fermi Gases with Two-Dimensional Spin-Orbit Coupling*, Phys. Rev. Lett. **117**, 235304 (2016).
- [42] B.-Z. Wang, Y.-H. Lu, W. Sun, S. Chen, Y. Deng, and X.-J. Liu, *Dirac-, Rashba- and Weyl-Type Spin-Orbit Couplings: Toward Experimental Realization in Ultracold Atoms*, Phys. Rev. A **97**, 011605(R) (2018)
- [43] S.-C. Ji, J.-Y. Zhang, L. Zhang, Z.-D. Du, W. Zheng, Y.-J. Deng, H. Zhai, S. Chen, and J.-W. Pan, *Experimental Determination of the Finite-Temperature Phase Diagram of a Spin-Orbit Coupled Bose Gas*, Nat. Phys. **10**, 314 (2014).
- [44] See supplementary material for more details.
- [45] J.-S. Pan, W. Zhang, W. Yi, and G.-C. Guo, *Bose-Einstein Condensate in an Optical Lattice with Raman-Assisted Two-Dimensional Spin-Orbit Coupling*, Phys. Rev. A **94**, 043619 (2016).
- [46] X.-J. Liu, K. T. Law, T. K. Ng, and P. A. Lee, *Detecting Topological Phases in Cold Atoms*, Phys. Rev. Lett. **111**, 120402 (2013).
- [47] B. Song, C. He, S. Zhang, E. Hajiyevev, W. Huang, X.-J. Liu, and G.-B. Jo, *Spin-Orbit-Coupled Two-Electron Fermi Gases of Ytterbium Atoms*, Phys. Rev. A **94**, 061604(R) (2016).
- [48] N. Q. Burdick, Y. Tang, and B. L. Lev, *Long-Lived Spin-Orbit-Coupled Degenerate Dipolar Fermi Gas*, Phys. Rev. X **6**, 031022 (2016).
- [49] P. Amara, D. Hsu, and J. E. Straub, *Global energy minimum searches using an approximate solution of the imaginary time Schroedinger equation*, J. Phys. Chem. **97**, 6715 (1993).
- [50] R. Grimm, M. Weidemajller, and Y. B. Ovchinnikov, *Optical dipole trap for neutral atoms*, in Adv. At. Mol. Opt. Phys. **42**, 95-170 (2000).